REFERENCES AND NOTES

1. L. Vesterlund, in *The Nonprofit Sector*, R. Steinberg, W. W. Powell, Eds. (Yale Univ. Press, New Haven, CT, ed. 2, 2006).
2. D. Rondeau, J. A. List, *Exp. Econ.* **11**, 253–267 (2008).
3. J. A. List, D. Lucking-Reiley, *J. Polit. Econ.* **110**, 215–233 (2002).
4. J. Andreoni, *J. Polit. Econ.* **106**, 1186–1213 (1998).
5. R. Croson, J. Shang, *Exp. Econ.* **11**, 221–233 (2008).
6. B. S. Frey, S. Meier, *Am. Econ. Rev.* **94**, 1717–1722 (2004).
7. J. Potters, M. Sefton, L. Vesterlund, *Econ. Theory* **33**, 169–182 (2007).
8. C. E. Cryder, G. Loewenstein, H. Seltman, *J. Exp. Soc. Psychol.* **49**, 1078–1083 (2013).
9. L. Vesterlund, *J. Public Econ.* **87**, 627–657 (2003).
10. C. C. Eckel, P. J. Grossman, *J. Public Econ.* **87**, 681–701 (2003).
11. C. C. Eckel, P. J. Grossman, *Nonprofit Volunt. Sector Q.* **33**, 271–289 (2004).
12. C. C. Eckel, P. J. Grossman, R. M. Johnston, *J. Public Econ.* **89**, 1543–1560 (2005).
13. D. Karlan, J. A. List, *Am. Econ. Rev.* **97**, 1774–1793 (2007).
14. S. Meier, *J. Eur. Econ. Assoc.* **5**, 1203–1222 (2007).
15. W. P. Barrett, Most charitable bang for the donor's buck. *Forbes*, 30 November 2011; www.forbes.com/sites/williampbarrett/2011/11/30/most-charitable-bang-for-the-donors-buck-2/.
16. J. Baron, E. Szymanska, in *The Science of Giving: Experimental Approaches to the Study of Charity*, D. M. Oppenheiemer, C. Y. Olivola, Eds. (Psychology Press, New York, 2011), chap. 13.
17. L. Caviola, N. Faulmüller, J. A. C. Everett, J. Savulescu, G. Kahane, *Judgm. Decis. Mak.* **9**, 303–316 (2014).
18. D. Tinkelman, K. Mankaney, *Nonprofit Volunt. Sector Q.* **36**, 41–64 (2007).
19. A. G. Gregory, D. Howard, *Stanford Soc. Innovation Rev.* **Fall**, 49–53 (2009).
20. J. D. Lecy, E. A. M. Searing, *Nonprofit Volunt. Sec. Q.* 10.1177/0899764014527175 (2014).
21. K. Wing, M. A. Hager, "Getting what we pay for: Low overhead limits nonprofit effectiveness," *Brief No. 3* (The Urban Institute, Washington, DC, 2004).
22. T. H. Pollak, "What we know about overhead costs in the nonprofit sector," *Brief No. 1* (The Urban Institute, Washington, DC, 2004).
23. K. Wing, M. A. Hager, "The quality of financial reporting by nonprofits: Findings and implications," *Brief No. 4* (The Urban Institute, Washington, DC, 2004).
24. M. A. Hager, T. Flack, "The pros and cons of financial efficiency standards," *Brief No. 5* (The Urban Institute, Washington, DC, 2004).
25. W. Bowman, *Nonprofit Volunt. Sector Q.* **35**, 288–310 (2006).
26. R. Steinberg, in *The Economics of Non Profit Institutions: Studies in Structure and Policy*, S. Rose-Ackerman, Ed. (Oxford Univ. Press, New York, 1986), pp. 347–364.
27. R. Bekkers, P. Wiepking, *Nonprofit Volunt. Sector Q.* **40**, 924–973 (2011).
28. R. Thaler, *J. Econ. Behav. Organ.* **1**, 39–60 (1980).
29. B. Duncan, *J. Public Econ.* **88**, 2159–2180 (2004).
30. As is common in running experiments with organizations, we signed a nondisclosure agreement that limits the amount of information we can give regarding the procedure.
31. J. Andreoni, *Econ. J.* **100**, 464–477 (1990).
32. A. Imas, *J. Public Econ.* **114**, 14–18 (2014).
33. G. A. Akerlof, R. E. Kranton, *Q. J. Econ.* **115**, 715–753 (2000).
34. D. Ariely, A. Bracha, S. Meier, *Am. Econ. Rev.* **99**, 544–555 (2009).
35. R. Bénabou, J. Tirole, *Am. Econ. Rev.* **96**, 1652–1678 (2006).
36. A. Gneezy, U. Gneezy, G. Riener, L. D. Nelson, *Proc. Natl. Acad. Sci. U.S.A.* **109**, 7236–7240 (2012).
37. A. Taylor, J. Harold, K. Berger, "The overhead myth: Letter to the donors of America" (2013); http://overheadmythcom.b.presscdn.com/wp-content/uploads/2013/06/GS_OverheadMyth_Ltr_ONLINE.pdf).
38. D. Pallotta, *Uncharitable: How Restraints on Nonprofits Undermine Their Potential* (Tufts Univ. Press, Lebanon, NH, 2008).

EARTH HISTORY

Low Mid-Proterozoic atmospheric oxygen levels and the delayed rise of animals

Noah J. Planavsky,[1]*† Christopher T. Reinhard,[2]*† Xiangli Wang,[1,3] Danielle Thomson,[4] Peter McGoldrick,[5] Robert H. Rainbird,[6] Thomas Johnson,[3] Woodward W. Fischer,[7] Timothy W. Lyons[8]

The oxygenation of Earth's surface fundamentally altered global biogeochemical cycles and ultimately paved the way for the rise of metazoans at the end of the Proterozoic. However, current estimates for atmospheric oxygen (O_2) levels during the billion years leading up to this time vary widely. On the basis of chromium (Cr) isotope data from a suite of Proterozoic sediments from China, Australia, and North America, interpreted in the context of data from similar depositional environments from Phanerozoic time, we find evidence for inhibited oxidation of Cr at Earth's surface in the mid-Proterozoic (1.8 to 0.8 billion years ago). These data suggest that atmospheric O_2 levels were at most 0.1% of present atmospheric levels. Direct evidence for such low O_2 concentrations in the Proterozoic helps explain the late emergence and diversification of metazoans.

I t remains unclear whether the appearance and diversification of animals are linked to a change in environmental oxygen (O_2) levels or if this dramatic shift in the structure and complexity of the biosphere simply reflects the timing of genetic and/or developmental innovation independent of any environmental control (*1–4*). Quantitative constraints on O_2 levels during the mid-Proterozoic [1.8 to 0.8 billion years ago (Ga)]—the long interval leading up to the Cambrian explosion in animal life (*5, 6*)—are required to compare atmospheric oxygen levels with the absolute O_2 requirements for metazoan physiology (*3, 5*). Such a comparison is essential for delineating the potential role of Earth's oxygen cycle in the early evolution of animal life.

The appearance of terrestrial red-beds and the disappearance of detrital pyrite beds indicate oxidative processes in terrestrial environments after ~2.4 Ga and a permanent rise in atmospheric O_2 concentrations above the very low values characteristic of the Archean atmosphere (<0.001% of the present atmospheric level or PAL) (*6, 7*). However, these observations provide only a crude lower estimate for mid-Proterozoic atmospheric O_2 of ~1% PAL. The most widely accepted upper limit on mid-Proterozoic atmospheric O_2 is ~40% PAL, which is an estimate based on the inferred temporal and spatial extent of anoxia in the Proterozoic ocean combined with steady-state physicochemical models of ocean ventilation (*8, 9*).

Chromium (Cr) isotopes may provide a much needed additional constraint on Proterozoic O_2 levels (*10*). Chromium exists in two primary redox states at Earth's surface—oxidized Cr(VI) and reduced Cr(III). Because Cr within the crust is hosted within rock-forming minerals predominantly as Cr(III), the initial Cr reservoir for terrestrial weathering will be stable under reducing conditions. In addition, Cr undergoes only limited fractionation during typical non-redox–dependent transformations (*11–13*), but the oxidation and reduction of Cr induce large isotope fractionations. At equilibrium, Cr(VI) species will be enriched in the heavy isotope, ^{53}Cr, by over 6‰ relative to the parent Cr(III) reservoir (*13*), although environmental fractionations are likely kinetic and are unlikely to reach this full equilibrium value (*12, 14*). Chromium oxidation occurs predominantly through the dissolution of Cr(III)-bearing minerals in terrestrial soils and subsequent reaction with manganese (Mn) oxides [e.g.,

---
[1]Department Geology and Geophysics, Yale University, CT, USA. [2]School of Earth and Atmospheric Sciences, Georgia Institute of Technology, GA, USA. [3]Department of Geology, University of Illinois, Champaign, IL, USA. [4]Department of Earth Science, Carleton University, Ottawa, ON, Canada. [5]Centre for Ore Deposit and Exploration Science, University of Tasmania, TAS, Australia. [6]Geological Survey of Canada, Ottawa, ON, Canada. [7]Division of Geological and Planetary Sciences, California Institute of Technology, Pasadena, CA, USA. [8]Department of Earth Sciences, University of California, Riverside, CA, USA.
*Corresponding author. E-mail: noah.planavsky@yale.edu (N.J.P.); chris.reinhard@eas.gatech.edu (C.T.R.) †These authors contributed equally to this work.

(15–17)], the occurrence of which in modern environments is linked specifically to the presence of free environmental O_2. This process yields dissolved Cr(VI) oxyanion species (CrO_4^{2-} and $HCrO_4^-$) that are significantly more soluble and mobile than Cr(III). However, during transport within and away from weathering environments, isotopically light Cr(VI) can be selectively reduced and immobilized (12, 14, 18). As a result, the net effect of redox reactions will be to produce a highly mobile CrO_4^{2-} reservoir with positive $\delta^{53}Cr$ values. In contrast, igneous systems are characterized by a very narrow range of Cr isotope ratios (reported as $\delta^{53}Cr$ values), with an average value of –0.12‰ (±0.101 2 SDs) (19). It is expected that the Cr cycle on a reducing Earth surface would be dominated by mobilization, transport, and burial of less mobile Cr(III) with minimal fractionation from igneous silicate Earth.

Although Cr isotope data have been used to examine the broad-scale oxygenation of Earth's atmosphere (10, 20), these initial surveys did not examine the billion-year interval before the evolution of animals. We targeted several mid-Proterozoic sedimentary successions to fill major gaps in the sedimentary Cr isotope record of this interval. To isolate redox conditions in terrestrial settings, we explored shallow, nearshore iron-rich marine units that are most likely to capture terrigenous weathering signals and lack measurable contributions from contemporaneous hydrothermal systems. We focused on samples from the 1.7-Ga Chuanlinggou Formation in China, the ~1.65-Ga Freedom Formation in the United States, the 1.45-Ga Sherwin Formation in Australia, and the ~0.9-Ga Aok Formation in Canada (21). The targeted samples comprise granular deposits that are sedimentologically and geochemically equivalent to Phanerozoic (<542-million-year-old) nearshore iron-rich deposits—rocks commonly referred to as ironstones (Fig. 1)—and formed in marginal marine or deltaic settings genetically similar to iron-rich portions of the modern Amazon delta (22). For comparison, we also determined the Cr isotope composition of a suite of analogous Phanerozoic ironstones, deposited between ~0.445 and 0.090 Ga, to provide a comparative view of Cr isotope systematics in nearshore iron-rich sedimentary units that formed beneath an atmosphere independently and unequivocally constrained to have been well-oxygenated.

Understanding petrographic context and postdepositional history is essential to interpret Cr isotope data. Chromium with either crustal or highly fractionated $\delta^{53}Cr$ values can be introduced into a rock unit during burial diagenesis, given that both oxidizing groundwaters and reduced basinal brines commonly lead to secondary metal enrichment [e.g., (23, 24)]. To gauge whether the examined samples record primary (depositional) or secondary Cr isotope signatures, we studied the samples using standard petrography and laser ablation–inductively coupled plasma mass spectrometry (LA-ICP-MS) trace-element mapping. Notably, the selected samples lack obvious textural or geochemical evidence for secondary mineralization. Chromium resides

predominantly in iron-rich sedimentary grains (e.g., concentrically coated iron ooids), rather than detrital Cr-rich grains (e.g., chromite) or diagenetic chemical cements (Fig. 2). This observation is consistent with Cr acquisition by sorption during sedimentation of precursor ferric oxides. In addition, preservation of fine-scale sedimentary textures in the ironstones, such as laminations in coated grains (Fig. 1 and fig. S1), is commonly observed and suggests limited fluid-rich alteration and recrystallization. Therefore, we are confident that our selected ironstone samples record depositional signals and thus can be used to track environmental Cr cycling.

All of the examined mid-Proterozoic ironstones have $\delta^{53}Cr$ values indistinguishable from those of igneous sources (–0.124‰, ±0.101 2 SDs, Fig. 2A). This range is in marked contrast to that of the examined Phanerozoic ironstones, which have consistently positive $\delta^{53}Cr$ values indicative of oxidative Cr cycling. Phanerozoic ironstone samples with a stronger detrital contribution have less-fractionated, near-igneous Cr isotopes values (Fig. 2A), which is an important factor controlling the

wide range of $\delta^{53}Cr$ values seen in Phanerozoic ironstones. In contrast, the mid-Proterozoic ironstones, despite being characterized by a broad range in authigenic Cr enrichment, show little to no isotopic offset from bulk silicate Earth—with no correlation between authigenic Cr enrichment and $\delta^{53}Cr$ values (Fig. 2A). This set of observations is most parsimoniously explained by the onset of a significant Cr(VI) exit channel from the terrestrial realm in the interval between the mid-Proterozoic and Phanerozoic data [e.g., (25)].

To test the hypothesis of a diminished Earth surface Cr redox cycling during mid-Proterozoic time, we sought an independent Cr archive in shales. Shales can also develop large authigenic Cr enrichments, marked by significantly higher Cr/Ti ratios than that of bulk crust. Authigenic Cr enrichment in fine-grained sediments and sedimentary rocks (shales) is thought to reflect processes similar to that in ironstones: coprecipitation and scavenging of particle-reactive Cr(III) phases or sorption and sequestration of dissolved Cr(VI) (26). Phanerozoic and latest Proterozoic shales commonly show large authigenic Cr
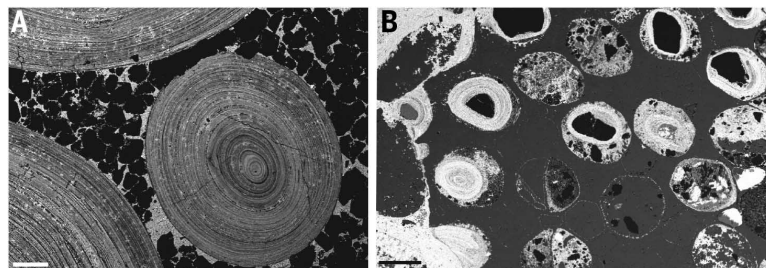
Fig. 1. Back-scatter electron micrographs of representative samples of ironstones. (**A**) the 1.45-Ga Sherwin Formation in northwestern Australia and (**B**) the 0.44-Ga Red Mountain Formation in southeastern United States. Samples are composed largely of hematite-coated grains and quartz sand. Fine concentric laminations of authigenic hematite are apparent. Scale bars, 200 μm.
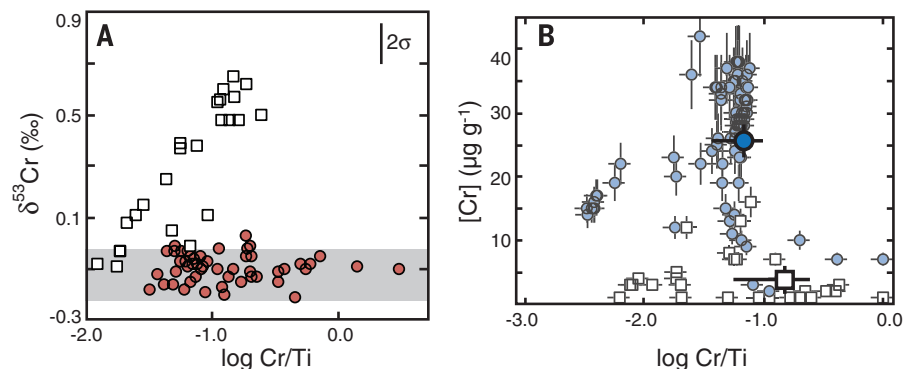
Fig. 2. Chromium isotope values and Cr/Ti ratios. (**A**) Phanerozoic (white squares) and Proterozoic (red circles) ironstones. The gray bar demarcates the igneous Cr isotope range, while the error bar in the top right denotes uniform external reproducibility (2σ). Phanerozoic and Proterozoic samples show a similar range in Cr/Ti ratios but markedly different Cr isotope trajectories. The trend defined by the Phanerozoic results from mixing between a crustal and an ^{53}Cr-enriched authigenic Cr component, providing a clear signal for an oxidative Cr cycle. (**B**) In situ Cr and Ti concentrations for representative mid-Proterozoic ironstones. Hematitic sedimentary grains are shown as blue circles; hematite cements, as white squares. Error bars in (B) denote uncertainty in measured concentrations of 15%, propagated into calculated Cr/Ti values (see supplementary materials). Large filled points denote the average values (±95% confidence interval) for grains (blue) and cements (white).

enrichments, whereas mid-Proterozoic shales are marked by Cr/Ti ratios similar to bulk crustal values (26). This relationship is consistent with widely reducing conditions and inventory drawdown in the earlier mid-Proterozoic ocean and/or smaller terrestrial-to-marine Cr fluxes (26). We observe a large range of δ^{53}Cr values for Phanerozoic-age Cr-enriched shales (Fig. 3). Most notably, we also find an increase in Cr enrichment and a wide range of δ^{53}Cr values in the ~0.8- to 0.75-Ga shales from the upper Wynniatt Formation in the Shaler Supergroup in Arctic Canada (27). The Wynniatt Formation yielded samples with markedly positive δ^{53}Cr values (peak values >2 ‰), which clearly indicate the operation of an oxidative surface Cr cycle at that time. The large Cr enrichments in these shales also suggest that a fully oxidative Cr cycle was in place (25, 26). Therefore, the coupled shale and ironstone record suggests that there was a major change in Cr cycling by at least 0.75 Ga.

We propose that the observed shifts in the shale and ironstone Cr records between ~0.8 and 0.75 Ga were caused by a rise in environmental

O_2 concentrations. Further, we suggest that the minimal Cr isotope fractionation observed during mid-Proterozoic time results from a general lack of Cr redox cycling. Although it is difficult to quantify the minimum amount of O_2 needed to induce and preserve large Cr isotope fractionations in marine chemical sediments, we estimate a range for this threshold by considering how ambient O_2 levels affect rates of Mn oxidation, which in turn affect Cr oxidation. Briefly, we use a kinetic model in which the relative amount of Cr(III) oxidation during weathering is governed by the availability of Mn(III,IV) species. Even with a wide range of ambient chemistries, Mn-oxide phases, and oxidation mechanisms (21), we find that extensive Mn-Cr redox cycling occurs at markedly low environmental O_2 levels (<0.1% PAL; Fig. 4). Thus, to explain the mid-Proterozoic Cr isotope data, we hypothesize that atmospheric partial oxygen pressure (pO_2) levels were at times, if not persistently, extremely low.

Minimum estimates for Proterozoic atmospheric pO_2 levels have been notoriously difficult to establish. Specifically, traditionally used lower

estimates for pO_2 values (>1% PAL), derived from paleosols (9), are likely to overestimate minimum atmospheric oxygen partial pressures due either to the use of extremely high [and likely incorrect; e.g., (28)] atmospheric CO_2 concentrations (in steady-state calculations) or because they neglect microbial iron oxidation (in kinetic-transport models). Further, there is a paucity of mid-Proterozoic paleosols (7), preventing direct, time-equivalent comparison between our results and the paleosol record. We note, however, previous suggestions on the basis of petrography and major-element geochemistry that the ~1.1-Ga Sturgeon Falls paleosol records a lack of terrestrial Mn oxidation—consistent with our Cr isotope data (29).

Others have suggested active environmental Cr redox cycling before our estimate of ~750 Ga (10, 20). Although each report must be evaluated individually, the presence of possible earlier periods of extensive Cr oxidation is consistent with atmospheric oxygen levels that were highly dynamic during the Precambrian and indicates that the traditional image of a unidirectional rise in atmospheric pO_2 is likely overly simplistic (30). Instability in atmospheric oxygen levels would be expected in a system characterized by very low O_2 partial pressures and thus potentially very short response times for the atmospheric oxygen reservoir. Dynamics aside, it seems clear that there is a first-order difference in the nature of Earth-surface Cr cycling between the mid-Proterozoic and the late-Proterozoic/Phanerozoic.

Under previous estimates of atmospheric pO_2 during the mid-Proterozoic (1% PAL < pO_2 < 40% PAL), there was potentially sufficient atmospheric oxygen for the earliest sessile and mobile animals to thrive well in advance of their ostensible emergence (3). However, our preferred maximum pO_2 estimate for mid-Proterozoic time
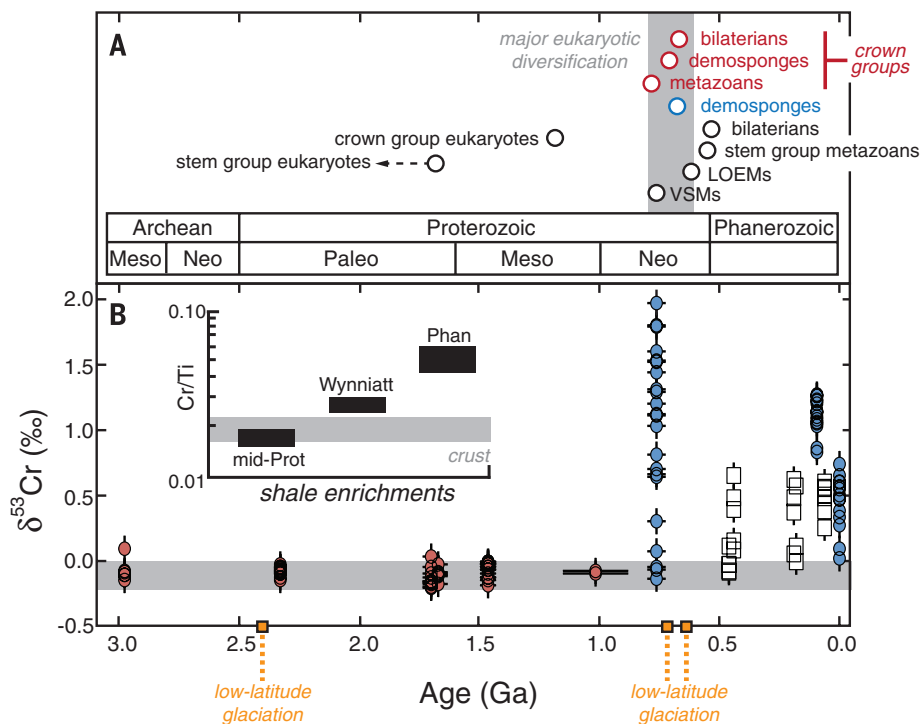
Fig. 3. Summary of sedimentary chromium isotope data in the context of major events in biological evolution. (A) Shown are approximate dates for the first appearance of various eukaryotic groups (2, 31, 32) in the body fossil record (open white circles), the molecular fossil record (open blue circle), and best estimates from molecular clock techniques for the emergence of major crown groups (open red circles). Also shown are the appearances of large ornamented Ediacaran microfossils (LOEMs) and vase-shaped microfossils (VSMs). The vertical gray field denotes an interval of major eukaryotic diversification. (B) Shown are Precambrian ironstone data (filled red circles), Phanerozoic ironstone data (white squares), and shale/mudstone data (filled blue circles) (n = 171). Horizontal gray field denotes the range for the isotopic composition of high-temperature Cr sources. Vertical error bars denote external reproducibility; horizontal error bars denote uncertainty in age constraints (error bars are smaller than symbol size when not shown). Inset shows a summary of the Cr enrichment record from anoxic shales, with boxes showing the average Cr/Ti value (±95% confidence interval) for each interval [data for mid-Proterozoic (mid-Prot) and Phanerozoic (Phan) from (26); data for the ~0.8- to 0.75-Ga Wynniatt Formation from this study]. Horizontal gray field in the inset denotes the range of Cr/Ti values for upper continental crust.
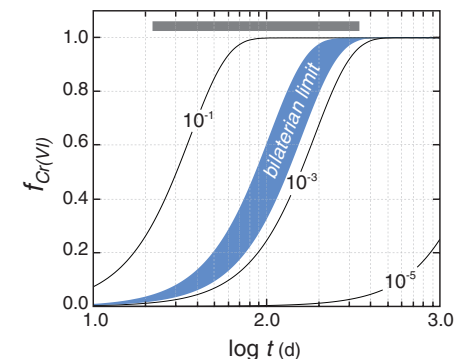
Fig. 4. Results from a kinetic model for Cr(III)-Mn(II) oxidation. Curves show the normalized fractional conversion of initial Cr(III) to Cr(VI) as a function of time in an oxidant-limited Mn-Cr system, with contours labeled according to atmospheric pO_2 (relative to the PAL). The blue field denotes values established from metabolic theory to be limiting for the last common ancestor of bilaterians (3), with the range encompassing organisms limited by pure diffusion and those that have a simple circulatory system. The dark gray bar shows an approximate range for the residence time of modern soil pore fluids.

(<0.1% PAL) is below theoretical estimates for the minimum O_2 requirements of the last common ancestor of bilaterians, measured limits at which bilaterians are found in the modern oceans, and threshold estimates for earlier diverging metazoan phyla (3, 4). In addition, it is possible that existing theoretical estimates of biological O_2 thresholds are biased toward low values, as they neglect the metabolic requirements of different life-history stages and synergistic physiological effects. In any case, our results suggest a temporal overlap between the appearance of stable environments favorable for animal life and the divergence of basal metazoan clades—which, according to recent estimates [e.g., (2)], occurred between ~0.8 and 0.7 Ga (Fig. 3). Though the emergence and eventual ecological dominance of animal life must, at its core, be tied to genetic and developmental innovations, our results implicate Earth's oxygen cycle as a crucial factor shaping the evolutionary landscape from which animal life emerged and help explain the delayed appearance of animals in the late Proterozoic.

REFERENCES AND NOTES

1. N. J. Butterfield, *Geobiology* **7**, 1–7 (2009).
2. D. H. Erwin *et al.*, *Science* **334**, 1091–1097 (2011).
3. E. A. Sperling, G. P. Halverson, A. H. Knoll, F. A. Macdonald, D. T. Johnston, *Earth Planet. Sci. Lett.* **371-372**, 143–155 (2013).
4. D. B. Mills *et al.*, *Proc. Natl. Acad. Sci. U.S.A.* **111**, 4168–4172 (2014).
5. J. L. Payne *et al.*, *Photosynth. Res.* **107**, 37–57 (2011).
6. H. D. Holland, *Philos. Trans. R. Soc. Lond. B Biol. Sci.* **361**, 903–915 (2006).
7. R. Rye, H. D. Holland, *Am. J. Sci.* **298**, 621–672 (1998).
8. D. E. Canfield, *Annu. Rev. Earth Planet. Sci.* **33**, 1–36 (2005).
9. L. R. Kump, *Nature* **451**, 277–278 (2008).
10. R. Frei, C. Gaucher, S. W. Poulton, D. E. Canfield, *Nature* **461**, 250–253 (2009).
11. A. S. Ellis, T. M. Johnson, T. D. Bullen, *Environ. Sci. Technol.* **38**, 3604–3607 (2004).
12. T. M. Johnson, T. D. Bullen, in *Geochemistry of Non-Traditional Stable Isotopes* (Mineralogical Society of America, Chantilly, VA, 2004), vol. 55, chap. 9, pp. 289–318.
13. E. A. Schauble, G. R. Rossman, H. P. J. Taylor Jr., *Chem. Geol.* **205**, 99–114 (2004).
14. S. Zink, R. Schoenberg, M. Staubwasser, *Geochim. Cosmochim. Acta* **74**, 5729–5745 (2010).
15. R. Bartlett, B. James, *J. Environ. Qual.* **8**, 31 (1979).
16. S. E. Fendorf, *Geoderma* **67**, 55–71 (1995).
17. J. Kotaś, Z. Stasicka, *Environ. Pollut.* **107**, 263–283 (2000).
18. A. S. Ellis, T. M. Johnson, T. D. Bullen, *Science* **295**, 2060–2062 (2002).
19. R. Schoenberg, S. Zink, M. Staubwasser, F. von Blanckenburg, *Chem. Geol.* **249**, 294–306 (2008).
20. S. A. Crowe *et al.*, *Nature* **501**, 535–538 (2013).
21. Materials and methods and full model details are available on *Science* Online.
22. R. C. Aller, J. E. Mackin, R. T. Cox Jr., *Cont. Shelf Res.* **6**, 263–289 (1986).
23. A. C. Brown, *Econ. Geol.* **100**, 765 (2005).
24. D. Leach *et al.*, *Econ. Geol.* **100**, 561 (2005).
25. K. O. Konhauser *et al.*, *Nature* **478**, 369–373 (2011).
26. C. T. Reinhard *et al.*, *Proc. Natl. Acad. Sci. U.S.A.* **110**, 5357–5362 (2013).
27. D. van Acken, D. Thomson, R. H. Rainbird, R. A. Creaser, *Precambrian Res.* **236**, 124–131 (2013).
28. N. D. Sheldon, *Precambrian Res.* **147**, 148–155 (2006).
29. E. A. Zbinden, H. D. Holland, C. R. Feakes, S. K. Dobos, *Precambrian Res.* **42**, 141–163 (1988).
30. T. W. Lyons, C. T. Reinhard, N. J. Planavsky, *Nature* **506**, 307–315 (2014).
31. G. D. Love *et al.*, *Nature* **457**, 718–721 (2009).
32. A. H. Knoll, *Cold Spring Harb. Perspect. Biol.* **6**, a016121 (2014).

CHEMICAL BIOLOGY

A bump-and-hole approach to engineer controlled selectivity of BET bromodomain chemical probes

Matthias G. J. Baud,[1,2]*† Enrique Lin-Shiao,[1,2]*‡ Teresa Cardote,[1]* Cynthia Tallant,[2]§ Annica Pschibul,[1] Kwok-Ho Chan,[1] Michael Zengerle,[1] Jordi R. Garcia,[1] Terence T.-L. Kwan,[2] Fleur M. Ferguson,[2] Alessio Ciulli[1,2]||

Small molecules are useful tools for probing the biological function and therapeutic potential of individual proteins, but achieving selectivity is challenging when the target protein shares structural domains with other proteins. The Bromo and Extra-Terminal (BET) proteins have attracted interest because of their roles in transcriptional regulation, epigenetics, and cancer. The BET bromodomains (protein interaction modules that bind acetyl-lysine) have been targeted by potent small-molecule inhibitors, but these inhibitors lack selectivity for individual family members. We developed an ethyl derivative of an existing small-molecule inhibitor, I-BET/JQ1, and showed that it binds leucine/alanine mutant bromodomains with nanomolar affinity and achieves up to 540-fold selectivity relative to wild-type bromodomains. Cell culture studies showed that blockade of the first bromodomain alone is sufficient to displace a specific BET protein, Brd4, from chromatin. Expansion of this approach could help identify the individual roles of single BET proteins in human physiology and disease.

The Bromo and Extra-Terminal (BET) proteins Brd2, Brd3, Brd4, and Brdt play key roles in transcriptional regulation by controlling networks of genes involved in cellular proliferation and cell-cycle regulation as part of multiprotein complexes. Misregulation of BET protein activity has been linked to disease states, notably in NUT-midline carcinoma and other cancers (1). Key to the activity of BET proteins are paired, highly homologous bromodomains present in their amino-terminal regions (Fig. 1A) that direct recruitment to nucleosomes by specifically binding to acetylated lysines within histone tails. Elucidation of the complex biological processes controlled by BET proteins would benefit greatly from chemical probes that allow perturbation of individual bromodomains with high selectivity.

Potent cell-active small molecules based on a triazolodiazepine scaffold including I-BET (2), JQ1 (3), and GW841819X (4) (Fig. 1B) were recently discovered that bind to the acetyl-lysine (KAc) binding pocket of BET bromodomains [dissociation constant (K_d) 50 to 370 nM for I-BET] (Fig. 1C, table S1, and fig. S1). These molecules display activity in vivo (5) against NUT-midline carcinoma (6), multiple myeloma (7), mixed-lineage leukemia (8), and acute myeloid leukemia (9,10). Several compounds, including I-BET, are now in clinical trials (11). These and other inhibitors developed to date are pan-selective for the BET members relative to other bromodomains (3) but show poor selectivity within the subfamily (Fig. 1C). Lack of selectivity confounds association of the pharmacology of BET bromodomain inhibitors to a particular target, which has fueled interest in finding more selective inhibitors. However, it is not clear which BET bromodomains should be

[1]Division of Biological Chemistry and Drug Discovery, College of Life Sciences, University of Dundee, James Black Centre, Dow Street, Dundee, DD1 5EH, UK. [2]Department of Chemistry, University of Cambridge, Lensfield Road, Cambridge CB2 1EW, UK.
*These authors contributed equally to this work. †Present address: Medical Research Council Laboratory of Molecular Biology, Francis Crick Avenue, Cambridge Biomedical Campus, Cambridge CB2 0QH, UK. ‡Present address: Biochemistry and Molecular Biophysics Graduate Group, Perelman School of Medicine, University of Pennsylvania, Philadelphia, PA 19104, USA. §Present address: Nuffield Department of Clinical Medicine, Structural Genomics Consortium, University of Oxford, Old Road Campus, Roosevelt Drive, Oxford OX3 7DQ, UK. ||Corresponding author. E-mail: a.ciulli@dundee.ac.uk